Statistical properties and stability of hot nuclei in a semiclassical relativistic approach

M. Rashdan
Department of Mathematics and Theoretical Physics, Atomic Energy Authority, Cairo, Egypt
(Received 27 January 1993)

Within the finite-temperature relativistic mean field theory models (linear and nonlinear) and using the local density approximation, the statistical properties and stability of hot nuclei are investigated. It is found that the nonlinear model presents higher thermal response than the linear model. The critical temperature is found to be about 9 MeV for the linear model and about 8 MeV for the nonlinear one. The value of the energy level density parameter obtained by the nonlinear model is found to be of the order of 0.11 MeV^{-1}, in good agreement with the empirical value $\simeq 0.12$ MeV^{-1}. The linear model gives smaller values. The nonrelativistic limit of the linear model indicates that the relativistic treatment increases the excitation.

PACS number(s): 21.65.+f

I. INTRODUCTION

A consistent nuclear equation of state for finite nuclei is of great utility for interpreting current experiments in heavy-ion scattering and high-energy particle-nucleus collisions. A necessary and major step towards obtaining this equation of state involves solving for the thermal properties of nuclei. Several calculations of thermal properties for finite nuclei through different nonrelativistic equations of state have been carried out [1–15]. For example, Bonche *et al.* [9] have used Skyrme-type interactions to study thermal properties and stability of excited nuclei in the framework of the finite temperature Hartree-Fock approach and they found that the results are very sensitive to the various versions of the Skyrme-type interactions. The critical temperature (the temperature beyond which the nuclei become unstable) has been found to be about 8 MeV and about 11 MeV for SKM and SIII Skyrme interactions. The energy level density parameter was found to be smaller than the empirical value for almost all Skyrme-type interactions. In a previous work [1] we also studied these thermal properties through the hot Thomas-Fermi approach using a realistic effective Brueckner *G*-matrix interaction obtained by solving the Bethe-Goldstone equation in momentum space at zero temperature using the Reid soft-core potential as a bare nucleon-nucleon interaction. We got a higher thermal response than the calculations of Bonche *et al.* The critical temperature was found not to exceed 6 MeV, while the energy level density parameter was found to be higher than the empirical value for light and medium nuclei and slightly smaller for the heavy ones. This shows that the thermal properties and stability of hot nuclei still need further investigations. Indeed, it would be interesting to treat this problem through the relativistic approaches. The relativistic field theory models provide a very useful tool in describing nuclear and neutron matters at a wide range of densities and temperatures. Thus one can use these models for the investigation of the thermal properties and stability of finite nuclei. For this reason, the linear Walecka model [16–20] and the nonlinear Boguta and Bodmer versions [21] are used in the mean-field approximation. These models consist of nucleons interacting via meson exchanges. The mean-field approximation treats the meson fields as classical *c*-number fields. Its effect is that the nucleons interact only via the mean fields. Thus the only quantum field is the nucleon field. However, the inclusion of the whole Dirac sea yields a divergent term in the energy which has to be canceled with counterterms. Another way for treating the negative and the positive continuum is to take a cutoff. However, using a cutoff has the liberating side effects that renormalizability is no longer a criterion for the ansatz of a model Lagrangian. Since at normal nuclear densities and not too high temperatures, which is the case of interest of this work, most of the quantum field effects are very small, one can use the no-sea approximation. Indeed, the effective Lagrangian is supposed to have absorbed all "leftover" quantum field effects in its parametrization. In the application of the mean-field models to finite nuclei, the local density approximation is used in the framework of the hot Thomas-Fermi approach. Moreover, surface and symmetry energy correction terms are added to the free energy in order to reproduce the experimental binding and root-mean-square (rms) radii at zero temperature. In Sec. II the equations of the finite-temperature relativistic mean-field theory models used in this work are presented. A nonrelativistic limit of the linear model is performed. The application of these mean-field models to finite nuclei through the hot Thomas-Fermi approach is described in Sec. III. Section IV presents the results and discussion.

II. FINITE-TEMPERATURE RELATIVISTIC MEAN-FIELD THEORY MODELS

In this section a brief description of the finite-temperature linear Walecka model and nonlinear Boguta and Bodmer versions is presented, and where it is assumed that the nucleons interact via the exchange of a scalar σ and a vector ω mesons. The relativistic classical Lagrangian density of a self-interacting scalar field ϕ and

a neutral vector field V_λ interacting with the nucleons is given by [16–21] ($\hbar=c=1$)

$$\mathcal{L}=-\bar{\psi}\left[\gamma_\lambda\frac{\partial}{\partial x_\lambda}+M\right]\psi-\frac{1}{2}\left[\left[\frac{\partial\varphi}{\partial x_\lambda}\right]^2+\mu^2\varphi^2\right]$$
$$-\tfrac{1}{4}F_{\lambda\mu}F_{\lambda\mu}-\tfrac{1}{2}m^2V_\lambda V_\lambda+ig_V\bar{\psi}\gamma_\lambda\psi V_\lambda-g_S\bar{\psi}\psi\varphi$$
$$-(\tfrac{1}{3}B\varphi^3+\tfrac{1}{4}C\varphi^4)\ . \tag{2.1}$$

The abbreviation $x=(r,it)$ is used. $F_{\lambda\mu}$ is the field stress tensor:

$$F_{\lambda\mu}=(\partial V_\mu/\partial x_\lambda)-(\partial V_\lambda/\partial x_\mu)\ . \tag{2.2}$$

M is the nucleon mass and m and μ are the masses of the vector and scalar mesons, respectively. The meson fields are treated classically and they are determined by their sources.

For infinite homogeneous systems, particle momentum and the corresponding energy are good quantum numbers. Using these together with the spin and isospin index, the fermion field is quantized. The spectral representation of the field ψ_k (k denotes all the quantum numbers) is determined from the requirement that the Gibbs free energy G be stationary. For finite-temperature nuclear matter G involves the particle occupation density operator $\hat{\rho}$. The state vectors ψ_k, scalar ϕ, vector field V_λ, and the density operator $\hat{\rho}$ are determined from the stationary condition of the Gibbs function, $\delta G=0$, with respect to arbitrary variations in these quantities under the constraints $\langle\psi_k,\psi_k\rangle=1$ and $\mathrm{Tr}\hat{\rho}=1$. This method is explained in Ref. [20]. For infinite homogeneous nuclear matter, the following expression for the energy density is obtained in the no-sea approximation:

$$\epsilon(\rho,T)=M^*\rho_S+k_e+\tfrac{1}{2}g_V^2\rho^2/m^2$$
$$+\tfrac{1}{2}g_S^2\rho_S[\rho_S+\beta M(M-M^*)^2-\gamma(M-M^*)^3]/\mu^2$$
$$+\tfrac{1}{6}\beta M(M-M^*)^3-\tfrac{1}{4}\gamma(M-M^*)^4\ , \tag{2.3}$$

where

$$k_e=\frac{g}{(2\pi)^3}\int d^3k\frac{k^2}{E_k}n_k\ . \tag{2.4}$$

The density ρ and the scalar density ρ_S are given by

$$\rho=\frac{g}{(2\pi)^3}\int d^3kn_k\ , \tag{2.5}$$

$$\rho_S=\frac{g}{(2\pi)^3}\int d^3k\frac{M^*}{E_k}n_k\ , \tag{2.6}$$

where

$$E_k=\sqrt{M^{*2}+k^2}\ . \tag{2.7}$$

The occupation probability n_k is given by

$$n_k=1/\{1+\exp[(E_k+g_V^2\rho/m^2-\lambda)/T]\}\ . \tag{2.8}$$

The effective mass M^* is determined self-consistently from

$$M^*=M-g_S^2[\rho_S+\beta M(M-M^*)^2-\gamma(M-M^*)^3]/\mu^2\ . \tag{2.9}$$

In the no-sea approximation, the effects of vacuum polarization and baryon-antibaryon production are neglected. This would be acceptable for normal nuclear densities and not too high temperatures, which is the more interesting case of this work. The parameters β ($=B/(Mg_S^3)$) and γ ($=C/g_S^4$) are introduced by Boguta and Bodmer [21].

In Ref. [20] a low and high temperature expansion has been considered for the densities (2.4)–(2.6) and a nonrelativistic limit has been performed on these expansions for the linear model. In this work, the exact expressions for these densities are used and a different nonrelativistic limit is performed. This limit is obtained by expanding E_k as follows:

$$E_k=\sqrt{M^{*2}+k^2}$$
$$=M^*+k^2/(2M^*)-k^4/(2M^*)^3+\cdots\ . \tag{2.10}$$

The third term of this expansion represents the first relativistic correction term. At zero temperature this term is taken into account in addition to the first two terms of the expansion (2.10) in the expressions of the densities k_e and ρ_S, given by Eqs. (2.4) and (2.6). At temperatures different from zero this term is neglected only in the expression of the occupation probability n_k, given by Eq. (2.8), in order to get the usual Fermi occupation probability:

$$n_k=1/\{1+\exp[(k^2/(2M^*)+g_V^2\rho/m^2-\lambda')/T]\}\ , \tag{2.11}$$

where

$$\lambda'=\lambda-M^*\ . \tag{2.12}$$

Figure 1 shows the binding energy per particle in nuclear matter against density at $T=0$ and 8 MeV. The solid curves represent the results of the linear model calculated with the parameters recently used by Furnstahl and Serot (LFS) [19] namely, $g_S^2M^2/\mu^2=357.4$, $g_V^2M^2/m^2=273.8$. The parameters β and γ only appear in the nonlinear model. The long-dashed curves represent the results of the nonlinear model calculated with Boguta and Bodmer (NLBB) [21] parameters, $g_S^2M^2/\mu^2=64$, $g_V^2M^2/m^2=4$, $\beta=0.471$, $\gamma=9.1$. With these parameters the binding energy is the same but at the saturation $\rho_0=0.149$ fm^{-3} for the LFS model and $\rho_0=0.171$ fm^{-3} for the NLBB model. Warke *et al.* [20] have used Walecka parameters [16] which give the same binding but at higher saturation $\rho_0=0.196$ fm^{-3}. The major difference between these models comes from the binding energy per particle as a function of density which is a very stiff curve for the linear model, while it is a very shallow curve for the nonlinear one, as seen from Fig. 1. The nonrelativistic limit described by Eqs. (2.10)–(2.12), which is performed for simplicity for the linear model, is shown in Fig. 1 by the short-dashed curves with the parameters of Furnstahl and Serot (NRLFS). It is shown

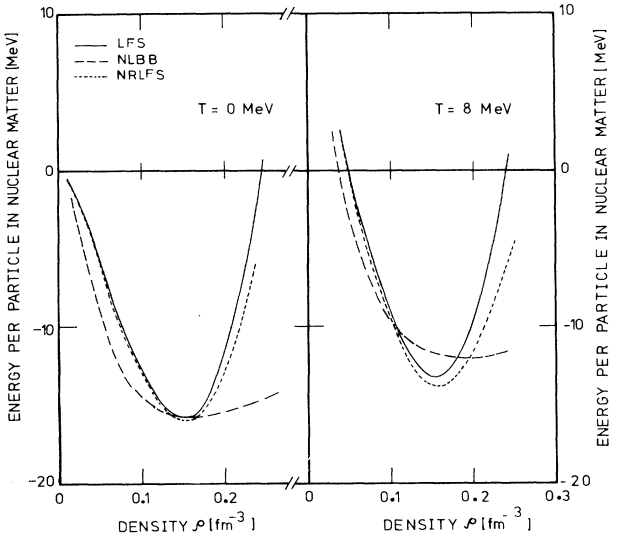

FIG. 1. The binding energy per particle in nuclear matter is plotted against density at $T=0$ and 8 MeV. The solid, long-dashed, and short-dashed curves represent the results of the linear model LFS, the nonlinear model NLBB, and the nonrelativistic limit of the linear model NRLFS.

that the relativistic response increases the excitation and the NLBB model has much larger excitation than the LFS model.

III. APPLICATION TO FINITE NUCLEI

The hot nuclear matter mean-field expressions (2.3)–(2.12) are applied to finite nuclei by using the local density approximation defined by Eq. (2.5). The total free energy of the nucleus is given by

$$F=E-TS\ , \tag{3.1}$$

where E and S are the total binding energy,

$$E=\int d^3r[(\epsilon(\rho,T)-M\rho)+\epsilon_{\rm cor}+\epsilon_{\rm Coul}]\ , \tag{3.2}$$

and the entropy,

$$S=\int d^3r\, s(\rho,T)\ . \tag{3.3}$$

The entropy density $s(\rho,T)$ is given by

$$s(\rho,T)=-\frac{g}{(2\pi)^3}\int d^3k[n_k\ln(n_k)+(1-n_k)\ln(1-n_k)]\ . \tag{3.4}$$

The nuclear matter mean-field energy density $\epsilon(\rho,T)$ appearing in Eq. (3.2) is given by Eqs. (2.3)–(2.9). $\epsilon_{\rm cor}$ is a correction term due to surface and symmetry energies and has the form [1,2,24]

$$\epsilon_{\rm cor}=\hbar^2/(8M)\chi(\nabla\rho)^2+\mathcal{D}(\rho_n-\rho_p)^2\rho^\nu,\quad \nu=-\tfrac{1}{3}\ , \tag{3.5}$$

where χ and $\mathcal{D}$ are two free parameters determined by minimizing the total binding energy E of the nucleus with respect to the density distribution parameters in order to get good agreement for binding energies and rms radii with the experimental values at zero temperature. However, theoretical investigations of the symmetry energy suggest that the symmetry energy coefficient $\mathcal{D}$ can be written as [22]

$$\mathcal{D}=\zeta e^{\alpha\nu},\quad -1\le\nu\le\tfrac{1}{3}\ , \tag{3.6}$$

where ζ equals 215 MeV fm^3 and e^α equals 9.39 fm^3 [22]. For ν equals $-\frac{1}{3}$, Eq. (3.6) gives the value 101.91 MeV fm^2 for $\mathcal{D}$. This value of $\mathcal{D}$ is taken in the present work for all nuclei. The last term in Eq. (3.2) is the Coulomb energy:

$$\epsilon_{\rm Coul}=\tfrac{1}{2}e^2\rho_p(r)\int d^3r'\frac{\rho_p(r')}{|r'-r|}-\tfrac{3}{4}(3/\pi)^{1/3}e^2\rho_p^{4/3}(r)\ . \tag{3.7}$$

IV. RESULTS AND DISCUSSION

The following form is taken for the density distributions ρ_i [23]:

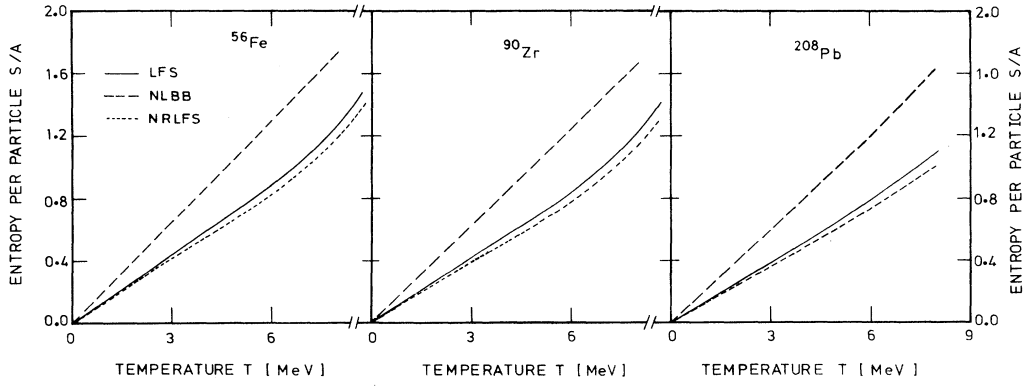

FIG. 2. The entropy per particle S/A for ^{56}Fe, ^{90}Zr, and ^{208}Pb is plotted against temperature T. The solid, long-dashed, and short-dashed lines represent the results of the LFS, NLBB, and NRLFS models.

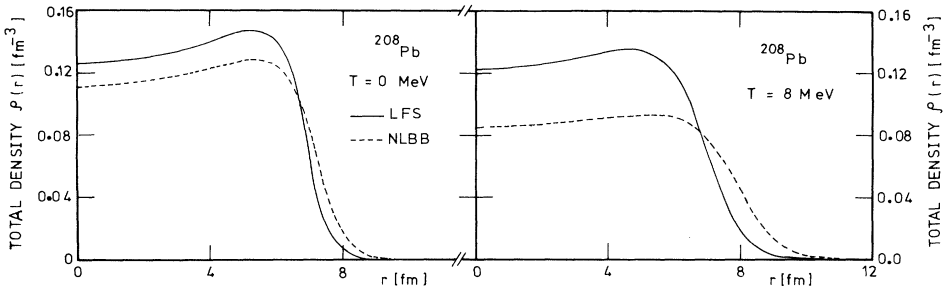

FIG. 3. The density distribution $\rho(r)$ $[=\rho_p(r)+\rho_n(r)]$ is plotted against r for ^{208}Pb at $T=0$ and 8 MeV. The solid and long-dashed curves represent the results of the LFS and NLBB models.

$$\rho_i=\frac{\rho_{0i}[1+\omega(r/R_i)^2]}{1+\exp[(r^2-R_i^2)/\alpha^2]},\quad i=p,n\ , \tag{4.1}$$

where ρ_{0i} is the central (proton or neutron) density of the nucleus. The distributions (4.1) are called the three-parameter Gaussian shape. This shape is taken in the present work for the nuclei ^{56}Fe, ^{90}Zr, and ^{208}Pb, since electron scattering experiments [23] favor these forms for these nuclei. The parameter ω is fixed from electron scattering experiments [23]. The neutron half-density radius is assumed to have the form

$$R_n=R_p+\delta R_0\ , \tag{4.2}$$

where

$$\delta=(N-Z)/A\ . \tag{4.3}$$

N, Z, and A are the neutron, charge, and mass numbers of the nucleus, respectively. R_0 is a length-scale parameter taken to be 1 fm. In a previous work [1,2,24] δ was taken to be 0.2 for the heavy nuclei. This value is consistent with the present approximation which is more general and directly relates the increase in the neutron radius to the increase in the neutron number of the nucleus. The central proton and neutron density distributions are determined from the normalization conditions

$$\int d^3r\,\rho_p(r)=Z,\quad \int d^3r\,\rho_n(r)=N\ . \tag{4.4}$$

At each finite value of the temperature T, the free energy F, defined by Eqs. (3.1)–(3.7), is minimized with respect to both the diffuseness and proton half-density radius parameters α and R_p of the nuclear density for each

TABLE I. The free energy per particle F/A, the binding energy per particle E/A, and the energy level density parameter a for ^{56}Fe, ^{90}Zr, and ^{208}Pb calculated at temperatures from 0 to 9 MeV for the linear model LFS (upper part) and at temperatures from 0 to 8 MeV for the nonlinear model NLBB (lower part).

	^{56}Fe			^{90}Zr			^{208}Pb		
T (MeV)	F/A (MeV)	E/A (MeV)	a (MeV^{-1})	F/A (MeV)	E/A (MeV)	a (MeV^{-1})	F/A (MeV)	E/A (MeV)	a (MeV^{-1})
				Linear model LFS					
0	−8.78	−8.78		−8.7	−8.7		−7.87	−7.87	
1	−8.83	−8.68	0.1	−8.73	−8.58	0.1	−7.93	−7.8	0.07
2	−9.03	−8.43	0.088	−8.94	−8.38	0.085	−8.1	−7.58	0.07
3	−9.43	−8.11	0.076	−9.31	−8.06	0.073	−8.43	−7.21	0.065
4	−9.97	−7.62	0.073	−9.82	−7.6	0.07	−8.89	−6.85	0.064
5	−10.63	−6.97	0.073	−10.44	−6.98	0.07	−9.47	−6.26	0.064
6	−11.44	−6.1	0.075	−11.21	−6.18	0.071	−10.18	−5.52	0.065
7	−12.41	−5.02	0.077	−12.12	−5.15	0.073	−11.03	−4.56	0.068
8	−13.58	−3.25	0.087	−13.22	−3.66	0.079	−12.04	−3.31	0.072
9	−14.96	−0.35	0.1	−14.6	−0.36	0.1			
				Nonlinear model NLBB					
0	−8.77	−8.77		−8.71	−8.71		−7.84	−7.84	
1	−8.91	−8.67	0.1	−8.83	−8.61	0.1	−7.97	−7.76	0.107
2	−9.21	−8.32	0.113	−9.13	−8.28	0.108	−8.25	−7.44	0.107
3	−9.73	−7.77	0.112	−9.63	−7.75	0.107	−8.73	−6.94	0.104
4	−10.53	−7.08	0.106	−10.39	−7.07	0.103	−9.45	−6.27	0.1
5	−11.49	−6.14	0.105	−11.31	−6.17	0.102	−10.34	−5.38	0.1
6	−12.67	−4.98	0.106	−12.45	−5.04	0.102	−11.44	−4.25	0.101
7	−14.06	−3.56	0.107	−13.79	−3.64	0.104	−12.74	−2.87	0.102
8	−15.68	−1.76	0.11	−15.35	−1.81	0.108	−14.27	−1.06	0.106

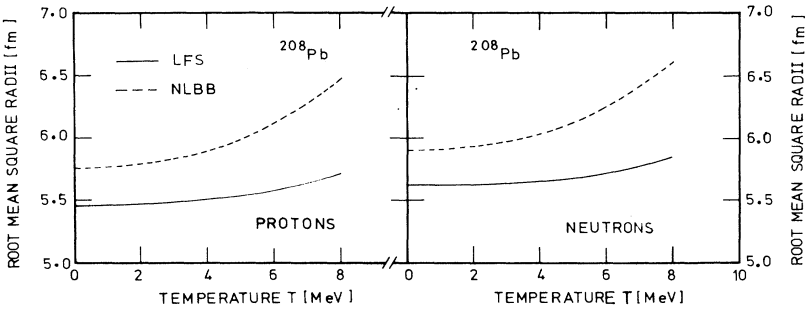

FIG. 4. Proton and neutron root-mean-square radii for ^{208}Pb are plotted against temperature T. The solid and long-dashed curves represent the results of the LFS and NLBB models.

nucleus. At the minimum, the free energy F, the binding energy E, the entropy S, the energy level density parameter a, and the root-mean-square radii are calculated. The energy level density parameter a is defined as

$$a = e^*/T^2 , \tag{4.5}$$

where e^* is the excitation energy per particle defined as

$$e^* = E^*/A , \tag{4.6}$$

where E^* is the difference between the binding energy of the nucleus calculated at T and the ground state energy, i.e.,

$$E^* = E(T) - E(0) . \tag{4.7}$$

At zero temperature, the value obtained for the surface correction parameter χ is found to be 8.5 fm^3 for ^{56}Fe and ^{90}Zr and slightly increased to 8.7 fm^3 for ^{208}Pb in the linear model LFS, while it is found in the nonlinear model NLBB to take the constant value 11.75 fm^3 for the three nuclei. χ is taken to be temperature independent.

Table I presents the results of the free energy per particle F/A, the binding energy per particle E/A, and the energy level density parameter a for ^{56}Fe, ^{90}Zr, and ^{208}Pb, at temperatures from 0 to 9 MeV for the LFS model, and from 0 to 8 MeV for the NLBB model. As seen from this table the free energies increase, and the binding energies decrease with increasing temperature. The NLBB model presents more excitation than the LFS model. This is due to the greater excitation that occurs in the binding energy per particle in nuclear matter in the case of the NLBB model, than that in the LFS model as shown from Fig. 1.

The entropy gets larger in the case of the NLBB model. This is shown in Fig. 2 which presents the entropy per particle S/A against temperature for ^{56}Fe, ^{90}Zr, and ^{208}Pb. The solid and long-dashed lines in this figure represent, respectively, the results obtained with the LFS and NLBB models. The short-dashed lines represent the results of the nonrelativistic limit of the linear model, NRLFS, described in Sec. II. This figure shows also that the relativistic entropy is larger than the nonrelativistic one.

The half-density radii and diffuseness and also the root-mean-square radii are increasing with increasing temperature. This is shown in Fig. 3, where the density distribution $\rho(r)$ $[=\rho_p(r)+\rho_n(r)]$ of ^{208}Pb is plotted against r at $T=0$ and 8 MeV, and in Fig. 4 where the proton and neutron root-mean-square radii are plotted against temperature. Again the solid and long-dashed curves represent, respectively, the results obtained with the LFS and NLBB models. The increases in the radii and diffuseness are much larger in the case of the NLBB model than in the LFS model. Similar results are obtained for the other two nuclei.

A more interesting quantity is the critical temperature T_c, the temperature beyond which the nucleus becomes unstable. As seen from Table I, T_c is a about 9 MeV for the LFS model, depending slightly on the nucleus, and about 8 MeV for the NLBB model. The difference comes from the larger excitation that occurs in the case of the NLBB model. In a previous nonrelativistic calculations based on the Brueckner G-matrix effective interaction [1], T_c was found not to exceed 6 MeV, while that obtained from the finite temperature Hartree-Fock calculations of Bonche *et al.* [9] was found to be about 8 MeV for SKM and about 11 MeV for SIII Skyrme interactions.

Another important quantity which can be deduced from experiments is the energy level density parameter a. This parameter has been found empirically to be of the order 0.12 MeV^{-1}. As seen from Table I a is around 0.07 MeV^{-1} for the LFS model and about 0.11 MeV^{-1} for the NLBB model. The value of a obtained from Hartree-Fock calculations with Skyrme interactions [5,6,9] has been found to be smaller than the empirical value, while that obtained from Brueckner G-matrix calculations [1] has been found to be much larger than the empirical value for light and medium nuclei and slightly smaller for the heavy ones. In these G-matrix calculations, the values of a have been obtained when the bare mass of the nucleon is used instead of the effective mass but if the effective mass is used [4], a is found to be close to the empirical value for light and medium nuclei and much smaller for the heavy ones. This means that a depends strongly on the effective mass of the nucleon. The energy level density parameter should also depend on the shell, pairing, and deformation effects. However, all these effects disappear at high excitations, $T > 3$ MeV [2], and a would mainly depend on the model equation of state.

It is a pleasure to thank Professor W. Wadia for reading the paper.

[1] M. Rashdan, A. Faessler, and W. Wadia, J. Phys. G **17**, 1401 (1991).
[2] A. Faessler, M. Rashdan, M. Ismail, N. Othsuka, and W. Wadia, Z. Phys. A **333**, 153 (1989).
[3] M. Rashdan, A. Faessler, M. Ismail, and N. Othsuka, Nucl. Phys. **A468**, 168 (1987).
[4] M. Rashdan, unpublished.
[5] G. Sauer, H. Chandra, and U. Mosel, Nucl. Phys. **A264**, 221 (1976).
[6] M. Barranco and J. Treiner, Nucl. Phys. **A351**, 269 (1981).
[7] M. W. Curtin, H. Toki, and D. K. Scott, Phys. Lett. **123B**, 289 (1983).
[8] G. Bozzoio and J. P. Vary, Phys. Rev. Lett. **53**, 903 (1984).
[9] P. Bonche *et al.*, Nucl. Phys. **A427**, 278 (1984); **A436**, 265 (1985); **A437**, 426 (1985).
[10] M. Brack, C. Guet, and H. Hakansson, Phys. Rep. **123**, 275 (1985).
[11] J. Okolwicz and J. M. Irvine, J. Phys. G **13**, 1399 (1987).
[12] A. Milian, M. Barranco, D. Mas, and R. J. Lombard, Z. Phys. A **330**, 5 (1988).
[13] F. Garcias, M. Barranco, J. Nemeth, and C. Ngo, Phys. Lett. B **206**, 177 (1988).
[14] C. Guet, E. Strumberger, and M. Brack, Phys. Lett. B **205**, 427 (1988).
[15] C. S. Wang, Phys. Rev. C **45**, 1084 (1992).
[16] J. D. Walecka, Phys. Lett. **59B**, 109 (1975).
[17] B. D. Serot and J. D. Walecka, Adv. Nucl. Phys. **16**, 1 (1986).
[18] L. W. Neise, H. Stoecker, and W. Greiner, J. Phys. G **13**, L181 (1987).
[19] R. J. Furnstahl and B. S. Serot, Phys. Rev. C **41**, 262 (1990).
[20] C. S. Warke, M. Uhlig, and W. Greiner, J. Phys. G **9**, 1083 (1983).
[21] J. Boguta and A. R. Bodmer, Nucl. Phys. **A292**, 413 (1977).
[22] J. Fink, U. Heinz, J. Maruhn, and W. Greiner, Z. Phys. A **323**, 189 (1986); J. Eisenberg and W. Greiner, *Nuclear Models* (North-Holland, Amsterdam, 1987), p. 743.
[23] C. W. De Jager *et al.*, At. Data Nucl. Data Tables **14**, 479 (1974).
[24] M. Rashdan, A. Faessler, N. Ohtuska, R. Linden, W. Wadia, and M. Ismail, Z. Phys. A **330**, 417 (1988).